Nanotechnology

PAPER

Effect of hydrogen on dynamic charge transport in amorphous oxide thin film transistors

To cite this article: Taeho Kim *et al* 2016 *Nanotechnology* **27** 325203

View the article online for updates and enhancements.

Related content

- Determination of intrinsic mobility of a bilayer oxide thin-film transistor by pulsed I–V method
  Hyunsuk Woo, Taeho Kim, Jihyun Hur et al.
- The influence of interfacial defects on fast charge trapping in nanocrystalline oxide-semiconductor thin film transistors
  Taeho Kim, Jihyun Hur and Sanghun Jeon
- Pulse I–V characterization of nano-crystalline oxide device with sub-gap density of states
  Taeho Kim, Ji-Hyun Hur and Sanghun Jeon

Recent citations

- A Sustainable Approach to Flexible Electronics with Zinc-Tin Oxide Thin-Film Transistors
  Cristina Fernandes *et al*
- Metal Composition and Polyethylenimine Doping Capacity Effects on Semiconducting Metal Oxide–Polymer Blend Charge Transport
  Wei Huang *et al*
- Electrical instability of high-mobility zinc oxynitride thin-film transistors upon water exposure
  Dae-Hwan Kim *et al*

IOP ebooks™

Bringing you innovative digital publishing with leading voices to create your essential collection of books in STEM research.

Start exploring the collection - download the first chapter of every title for free.

This content was downloaded from IP address 143.248.110.56 on 26/11/2019 at 08:31

IOP Publishing
Nanotechnology
Nanotechnology **27** (2016) 325203 (6pp)
doi:10.1088/0957-4484/27/32/325203

Effect of hydrogen on dynamic charge transport in amorphous oxide thin film transistors

Taeho Kim[1], Yunyong Nam[2], Ji-Hyun Hur[1], Sang-Hee Ko Park[2] and Sanghun Jeon[1]

[1] Department of Applied Physics, Korea University, Sejong, Korea
[2] Department of Materials Science and Engineering, KAIST, Daejeon, Korea

E-mail: shkp@kaist.ac.kr and jeonsh@korea.ac.kr

Received 25 March 2016, revised 3 June 2016
Accepted for publication 13 June 2016
Published 1 July 2016

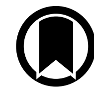

Abstract

Hydrogen in zinc oxide based semiconductors functions as a donor or a defect de-activator depending on its concentration, greatly affecting the device characteristics of oxide thin-film transistors (TFTs). Thus, controlling the hydrogen concentration in oxide semiconductors is very important for achieving high mobility and minimizing device instability. In this study, we investigated the charge transport dynamics of the amorphous semiconductor InGaZnO at various hydrogen concentrations as a function of the deposition temperature of the gate insulator. To examine the nature of dynamic charge trapping, we employed short-pulse current–voltage and transient current–time measurements. Among various examined oxide devices, that with a high hydrogen concentration exhibits the best performance characteristics, such as high saturation mobility (10.9 $cm^2 v^{-1} s^{-1}$), low subthreshold slope (0.12 V/dec), and negligible hysteresis, which stem from low defect densities and negligible transient charge trapping. Our finding indicates that hydrogen atoms effectively passivate the defects in subgap states of the bulk semiconductor, minimizing the mobility degradation and threshold voltage instability. This study indicates that hydrogen plays a useful role in TFTs by improving the device performance and stability.

Keywords: oxide semiconductor, charge transport, InGaZnO, hydrogen, defects

(Some figures may appear in colour only in the online journal)

Hydrogen in zinc oxide based semiconductors, represented by InGaZnO (IGZO), ZnSnO (ZTO) and InHfZnO (IHZO), have emerged as promising candidates for use in switching and driving devices in active-matrix liquid crystal displays as well as wearable devices owing to their strong advantages, such as large-area device integration, low-cost fabrication process and perfect process compatibility with previous display technologies, which stems from their outstanding electrical, material, and optical properties [1–5]. The amorphous structure in bulk semiconductors has a certain number of inherent subgap densities of states, which determine both the electrical characteristics and reliability [6–8]. In addition, because of the low-temperature process used in this technology, interfacial defects between the gate insulator and semiconductor exist in TFT devices, affecting the device mobility and stability [9, 10]. To obtain high mobility and high stability, various approaches to defect engineering have been introduced using various processes such as cation or anion optimization; oxygen vacancy manipulation; bi-, tri-, or multilayer adoption; and post photo/annealing processes [11–15]. However, precise control of defects in oxide semiconductor TFTs remains problematic owing to a significant number of subgap states in these semiconductors [16–20]. Thus, it is necessary to minimize defects in oxide TFTs as well as to understand their implications for device performance.

It is well known that hydrogen can be used to tune the electrical properties of oxide semiconductors [21–24]. It has a tendency to bond with oxygen in oxide semiconductors

 © 2016 IOP Publishing Ltd Printed in the UK

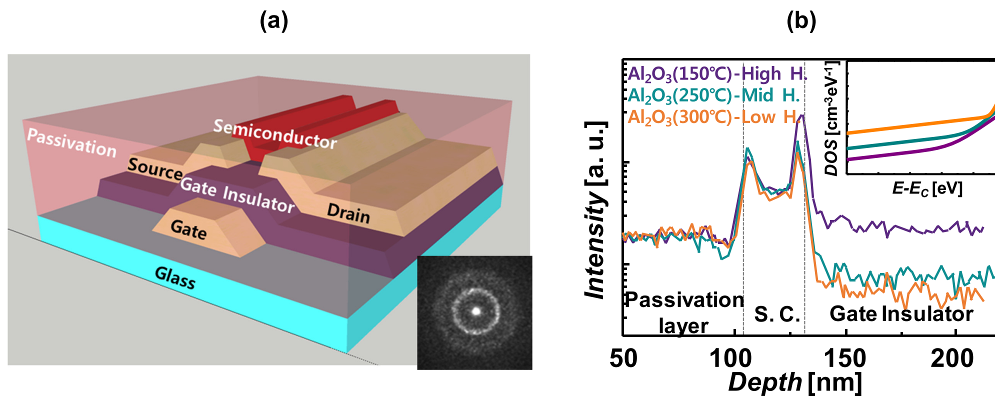

Figure 1. (a) Schematic structure of a bottom gate *a*-IGZO TFT. (b) Data of the SIMS depth profile for hydrogen concentration in *a*-IGZO with increasing Al_2O_3 deposition temperature. Inset shows density of states versus energy for Al_2O_3 stacked *a*-IGZO TFT with hydrogen concentration.

because of the very different electronegativities of these two elements [21–24]. Thus, hydrogen is always found in oxide semiconductors. It deactivates defects or generates shallow donors depending on the hydrogen concentration. When it forms bonds with oxygen and generates negatively charged hydroxide anions, hydrogen becomes a shallow donor in oxide semiconductors; consequently, a device becomes conductive and exhibits an insignificant on–off current ratio [21–24]. Very recently, however, various researchers have reported on beneficial effects of hydrogen, such as defect deactivation [25–27]. To date, however, the effect of hydrogen on defects in IGZO and on the TFT characteristics are not well examined or clearly understood. A critical reason is that the TFT characteristics are generally measured by conventional DC current–voltage ($I-V$) measurement, which provides an inherent charge-trapping environment due to the relatively long measurement time.

In this regard, microsecond-pulse I_D-V_G measurement is quite useful for minimizing the effects of fast charge trapping, which causes a few unfavorable characteristics, such as threshold voltage instability and underestimation of the mobility of transistors [28–32]. In comparison to conventional DC measurement, which takes a few seconds, the microsecond short-pulse I_D-V_G method takes a few microseconds to a few tens of microseconds, making it possible to minimize the effects of fast transient charging [28–32]. Consequently, the device characteristics can be measured under conditions with few or no charge traps, making it possible to evaluate the intrinsic device characteristics and to understand the dynamic charge transport on a time scale of microseconds [28–32].

In this paper, we examine the effect of the hydrogen concentration in oxide semiconductors on dynamic charge transport in oxide TFTs. To study the dynamic charge trapping and detrapping behavior as well as carrier transport mechanism, we employed microsecond short-pulse drain current−gate voltage (I_D-V_G) characterization and transient I_D–time measurements. We found that, in comparison to the mobility (μ) obtained by the DC I_D-V_G method, the channel μ values of TFTs obtained by fast pulse I_D-V_G measurement increased by 1.6%–121.1% depending on the hydrogen concentration in oxide semiconductors. In addition, our research results show that an oxide TFT with a high hydrogen concentration exhibits fewer defects and is less susceptible to ambient charge trapping, indicating that hydrogen plays a helpful role in defect passivation.

Bottom-gated TFTs of IGZO were fabricated using conventional thin film deposition, photolithography, and etching methods. A schematic diagram is presented in figure 1(a). A 40 nm thick IGZO thin film was prepared by radio-frequency sputtering using Ar and O_2 gases. The composition ratio of In, Ga and Zn of the IGZO film were 1, 1, and 2.5, respectively. The structure of the IGZO thin film was examined by transmission electron microscopy. The results revealed tiny bright dots with ring patterns in a hazy background (figure 1(a), inset), indicating that the IGZO semiconductor material is formed of an amorphous medium. This amorphous IGZO semiconductor is referred to as *a*-IGZO hereafter. For all the electrodes, thin films of the transparent conductor indium tin oxide were deposited to a thickness of 100 nm by radio-frequency sputtering using Ar gas. Atomic layer deposition of the dielectric material Al_2O_3 was performed using trimethylaluminum as the metal precursor and water as the reactant; this was followed by passivation and contact etching processes. The hydrogen concentration in *a*-IGZO was adjusted by increasing the deposition temperature of the Al_2O_3 gate insulator from 150 °C to 250 °C and 300 °C. For hydrogen diffusion step, we performed annealing process at 300 °C in vacuum. This is quite effective manner of hydrogen diffusion into oxide semiconductor [21]. Secondary ion mass spectrometry was used to examine the hydrogen concentration. As seen in figure 1(b), the hydrogen concentration in *a*-IGZO decreases with increasing Al_2O_3 deposition temperature. There is a tendency of hydrogen concentration in the front channel and front interface of Al_2O_3/IGZO as well as back interface of IGZO/SiO_2 with Al_2O_3 deposition temperature. The Al_2O_3 stacked *a*-IGZO TFT processed at 150 °C exhibits a higher hydrogen concentration in the front channel and front/back interface than the TFTs processed at 250 °C and 300 °C. The relative concentrations of hydrogen for three samples in order from highest to lowest were 2, 1.3, and 1.0 respectively. This

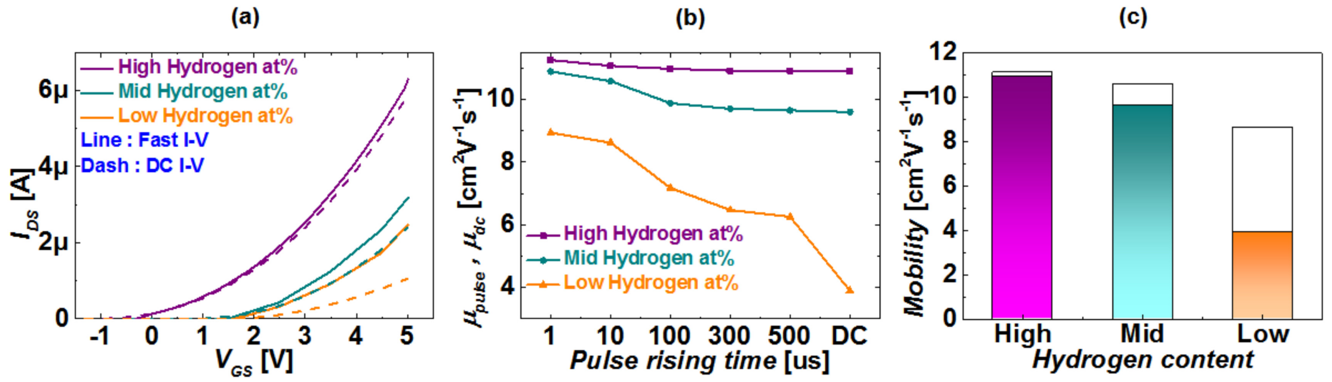

Figure 2. (a) Fast I_D-V_G and DC I_D-V_G transfer curves of *a*-IGZO TFTs with various hydrogen concentrations. (b) Mobility values of *a*-IGZO TFTs with various hydrogen concentrations obtained by fast I_D-V_G with respect to pulse rising time and DC I_D-V_G measurement techniques. (c) Mobility values of *a*-IGZO TFTs with various hydrogen concentrations obtained by fast I_D-V_G (white) and DC I_D-V_G measurement (colored) techniques.

difference also affects the subgap states in *a*-IGZO which were extracted by a multifrequency capacitance–voltage (*C*–*V*) characterization method [33, 34], as shown in the inset of figure 1(b). The *a*-IGZO TFT with a high hydrogen concentration shows lower subgap states than those with a low hydrogen concentration, indicating that hydrogen passivates the subgap states in *a*-IGZO [21]. Also Hall measurements data presents high hydrogen device presents high carrier concentration and high mobility in IGZO active layer, indicating that hydrogen plays in donor in oxide semiconductor.

To understand the effect of the hydrogen concentration in the *a*-IGZO semiconductor on the device characteristics of the *a*-IGZO TFT, we performed DC and microsecond fast-ramp I_D-V_G measurements using a semiconductor device parameter analyzer with a pulse generator and a high-resolution oscilloscope [28–32]. The DC I_D-V_G measurements were made at a scan speed of $4\ \mathrm{V\ s^{-1}}$, and the fast-ramp I_D-V_G measurements were made at a voltage ramping speed of $0.1-50\ \mu\mathrm{s\ V^{-1}}$. Figure 2(a) shows the DC and microsecond fast-ramp I_D-V_G curves (voltage rise time of 1 μs) of *a*-IGZO TFT devices with various hydrogen concentrations. The *a*-IGZO TFT with a high hydrogen concentration exhibits a high μ value ($17.9\ \mathrm{cm^2\ V^{-1}\ s^{-1}}$) and low subthreshold slope (*s*) (0.11 V/dec.), whereas those with intermediate and low hydrogen concentrations exhibit values of $\mu = 8.5\ \mathrm{cm^2\ V^{-1}\ s^{-1}}$ and $S = 0.17$ V/dec and $\mu = 2.2\ \mathrm{cm^2\ V^{-1}\ s^{-1}}$ and $S = 0.21$ V/dec respectively. High mobility characteristics of the *a*-IGZO TFT with a high hydrogen concentration can be explained by the combined effect of low defect and high carrier concentration. For all the tested devices, the microsecond fast-ramp I_D-V_G curves show a higher I_D level and steeper slope than the DC I_D-V_G curves. As seen in figure 2(b), the mobility values of the *a*-IGZO TFT device with a high hydrogen concentration decrease gradually with increasing voltage rise time, whereas those of the TFTs with intermediate and low hydrogen concentrations decrease significantly with increasing the ramp time. Figure 2(c) shows the μ values of *a*-IGZO TFTs with various hydrogen concentrations extracted from the DC and fast-ramp I_D-V_G curves. As expected, in agreement with figures 2(a) and (b), the μ values extracted from the fast-ramp I_D-V_G curves are higher than those taken from the DC I_D-V_G data, indicating that the effect of fast charge trapping can be suppressed in the fast-ramp I_D-V_G curve. Furthermore, the *a*-IGZO TFT with a low hydrogen concentration shows a significantly higher mobility increase rate ($\mu_{\text{fast-pulse}}/\mu_{DC}$) than that with a high hydrogen concentration, suggesting that the former is susceptible to fast charge trapping due to high subgap states in the semiconductor, as shown in the inset of figure 1(b). The μ values of the *a*-IGZO TFT devices with high, intermediate, and low hydrogen concentrations increased by 1.58%, 10.25%, and 121.1%, respectively, after the fast ramp I_D-V_G measurement.

To further understand the effect of the hydrogen concentration in *a*-IGZO semiconductors on the charge trapping and detrapping characteristics of *a*-IGZO TFT devices, the hysteresis characteristics were measured using microsecond short-pulse I_D-V_G curves at a pulse width of 2 ms. The test setup is illustrated in figure 3(a). Figure 3(b) shows the microsecond single-pulse I_D-V_G curves (obtained at a pulse rise/fall times of 1 μs and a pulse width of 4 ms) for three *nc*-IGZO TFTs. As shown on the left side of figure 3(b), we obtained two sets of I_D-V_G curves measured during the pulse rise/fall times. During the pulse fall time, the lower current level in the I_D-V_G data can be explained by fast charge trapping during the pulse duration [28–32]. During the pulse duration of 2 ms, the *a*-IGZO TFTs with high, intermediate, and low hydrogen concentrations exhibit ΔV_{th} values of 0.41, 1.58, and 3.34 V, indicating that 1.81×10^{11}, 6.94×10^{11}, and $1.59 \times 10^{12}\ \mathrm{cm^{-2}}$ carriers, respectively, were trapped in the subgap states in the semiconductor. The right side of figure 3(b) shows the transient I_D–time characteristics of *a*-IGZO TFT devices with various hydrogen concentrations, which illustrate fast transient charge trapping during the pulse duration. As the gate bias voltage in the gate pulse reached the plateau region, the I_D levels started to decrease. The reduction in the I_D levels was most noteworthy in the *a*-IGZO TFT with the low hydrogen concentration, suggesting that this device has a significant number of subgap defects in the interface and bulk oxide semiconductor as compared with the *a*-IGZO TFT with a high hydrogen concentration.

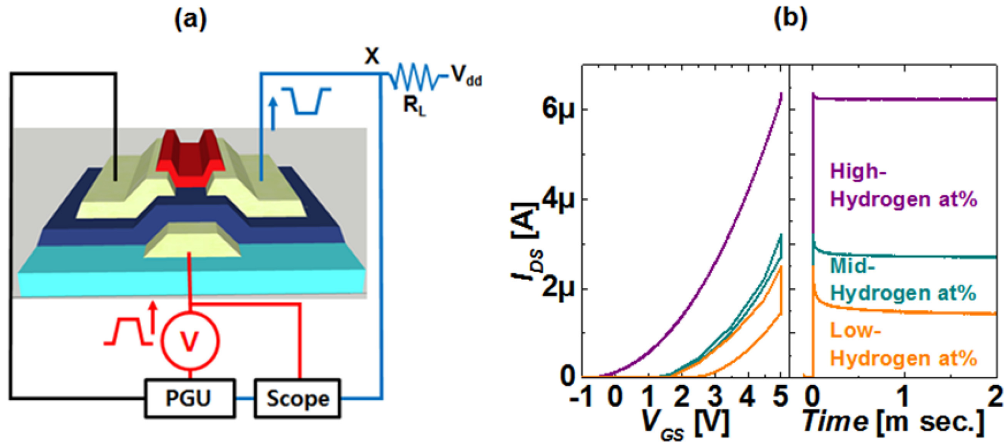

Figure 3. (a) Schematics of pulse I_D–V_G measurement system setup. (b) Pulse I_D–V_G curves and corresponding transient I_D–time data of *a*-IGZO TFTs with various hydrogen concentrations.

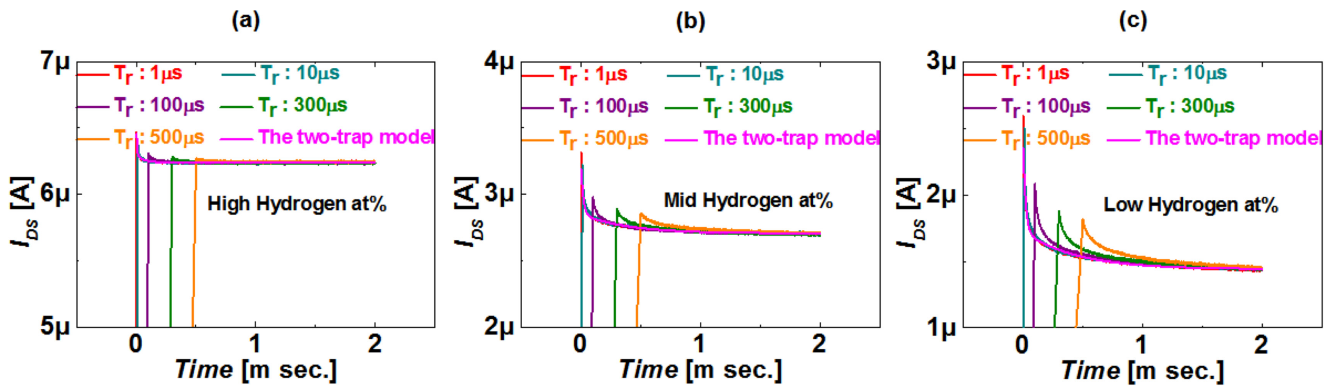

Figure 4. Transient I_D–time characteristics of *a*-IGZO TFTs with various hydrogen concentrations as a function of pulse rising time.

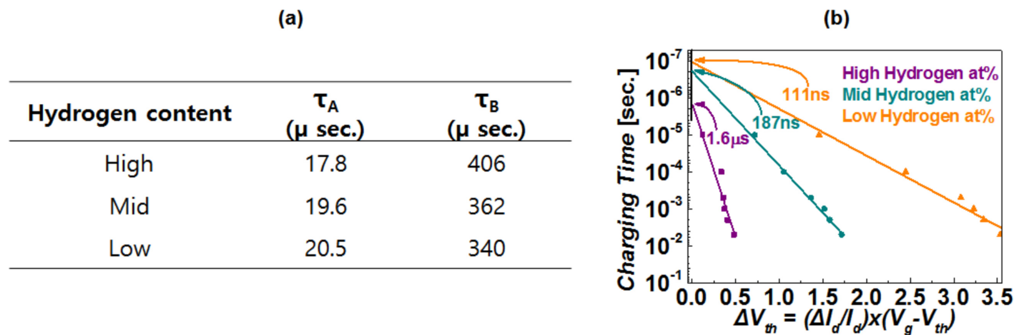

Hydrogen content	τ_A (μ sec.)	τ_B (μ sec.)
High	17.8	406
Mid	19.6	362
Low	20.5	340

Figure 5. (a) Time constants of *a*-IGZO TFTs with various hydrogen concentrations extracted from two trap fitting model. (b) ΔV_{th}-charging time of *a*-IGZO TFTs with various hydrogen concentrations.

To assess the dynamic charge trapping properties of the *a*-IGZO TFTs, we measured the transient I_D–time curves for rise times of 1–500 μs, as seen in figures 4(a)–(c). During the pulse duration, I_D decayed rapidly because of fast transient charge trapping, followed by gradual saturation within a few milliseconds. Then, I_D approached a certain value with a typical charge trapping curve. The measured transient I_D–time data were fitted with two-trap models using the equation $I = AI_o \exp(-t/\tau_A) + BI_o \exp(-t/\tau_B)$ with two time constants [35]. The best-fitted one and the measured data are presented in figures 4(a)–(c) for the *a*-IGZO TFTs with high, intermediate, and low hydrogen concentrations, respectively. The two-trap model for the *a*-IGZO TFTs with various hydrogen concentrations described well all the charge-trapping regions at the initial, intermediate, and long time scales. Note that the transient I_D variation with time obviously follows multiple trap-to-trap charging processes. Two different time constants for the *a*-IGZO TFTs are presented in figure 5(a). The shorter trap time constants (t_A) for three devices are similar while the longer trapping time constans (t_B) are significantly influenced by hydrogen concentration in oxide TFTs.

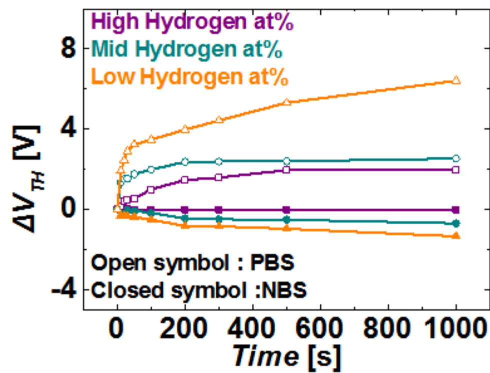

Figure 6. Positive bias stress (open symbol) and negative bias stress (closed symbol) characteristics of *a*-IGZO TFTs with various hydrogen concentrations.

To quantitatively analyze the trap time constant, we estimated the threshold voltage shift (ΔV_{th}) from the measured transient I_D–time data using the equation $\Delta V_{th} = \Delta I_D(V_G - V_{th})/I_D$, where ΔI_D is the difference between the I_D values at the initial and final points of the pulse duration, V_G is the pulse amplitude, V_{th} is the threshold voltage and I_D is the maximum drain current at the pulse onset [28–31]. The charging time versus ΔV_{th} is plotted for the *a*-IGZO devices with various hydrogen concentrations in figure 5(b). The critical trapping time constant (τ_C, the time at which charge trapping begins) can be estimated from the curve of the charging time versus ΔV_{th}. The *a*-IGZO TFT with a high hydrogen concentration exhibits a long τ_C of 1.6 μs, whereas the τ_C values of the *a*-IGZO TFTs with intermediate and low hydrogen concentrations are 187 and 111 ns, respectively.

To probe whether charge transport occurs primarily in the interface or the bulk, we measured the low-frequency noise (LFN). According to the normalized power spectral density S_{ID} versus $|V_{GS} - V_{th}|^{-x}$ for $x \sim 1.03$ (high hydrogen concentration), $x \sim 1.12$ (intermediate hydrogen concentration), and $x \sim 1.399$ (low hydrogen concentration), which are close to 1, carrier transport occurs mainly via the bulk channel [36–39]. Thus, hydrogen, which effectively deactivates bulk subgap states in semiconductors, improves the device performance and reliability of *a*-IGZO TFTs [36–39]. Therefore, as we determined in positive and negative bias stability (PBS and NBS) tests, (PBS, $V_G = 20$ V, $V_D = 0$ V, NBS: $V_G = -20$ V, $V_D = 0$ V), the *a*-IGZO TFT with a high hydrogen concentration exhibits a lower ΔV_{th} (figure 6), which is related to the subgap states in the front channel.

In this paper, we described the dynamic charge transport in *a*-IGZO TFTs with various hydrogen concentrations. To this end, we employed fast-ramp $I_D - V_G$, short-pulse $I_D - V_G$, and transient I_D−time measurements. Further, to probe the subgap states in *a*-IGZO, we applied multifrequency *C*–*V* and LFN methods. Among oxide TFTs with various hydrogen concentrations, the device with a high hydrogen concentration exhibited the best performance (high mobility and low subthreshold slope) and negligible charge trapping characteristics, which resulted from the low subgap states in *a*-IGZO. This indicates that the incorporation of hydrogen into *a*-IGZO deactivates the subgap defects in the bulk semiconductor, minimizing the mobility degradation and threshold voltage instability. This study demonstrates that hydrogen plays a useful role in improving the device performance and reliability of oxide TFTs. Therefore, controlling the hydrogen concentration is crucial for successful application of oxide TFTs.

Acknowledgments

This work was supported by the National Research Foundation of Korea (NRF) grant funded by the Korean Government (MEST) (No. 2014R1A2A2A01006541). This work was also supported in part by Samsung Display Co., Ltd. through the KAIST Samsung Display Research Center Program.

References

[1] Nomura K, Ohta H, Takagi A, Kamiya T, Hirano M and Hosono H 2004 Room-temperature fabrication of transparent flexible thin-film transistors using amorphous oxide semiconductors *Nature* **432** 488–92
[2] Kamiya T, Nomura K and Hosono H 2010 Present status of amorphous In–Ga–Zn-O thin film transistors *Sci. Technol. Adv. Mater.* **11** 044305
[3] Hosono H 2006 Ionic amorphous oxide semiconductors: Material design, carrier transport, and device application *J. Non-Cryst. Solids* **352** 851–8
[4] Jeon S *et al* 2012 Gated three-terminal device architecture to eliminate persistent photoconductivity in oxide semiconductor photosensor arrays *Nat. Mater.* **11** 301–5
[5] Martins R, Barquinha P, Pereira L, Ferreira I and Fortunato E 2007 Role of order and disorder in covalent semiconductors and ionic oxides used to produce thin film transistors *Appl. Phys.* A **89** 37–42
[6] Ahn S *et al* 2013 High-performance nanowire oxide photo-thin film transistor *Adv. Mater.* **25** 5549–54
[7] Choi H, Jeon S, Kim H, Shin J, Kim C and Chung U-I 2011 Influence of Hf contents on interface state properties in a-HfInZnO thin-film transistors with SiN_x/SiO_x gate dielectrics *Appl. Phys. Lett.* **99** 183502
[8] Jeon S, Beneyad A, Ahn S, Park S, Song I, Kim C and Chung U-I 2011 Short channel device performance of amorphous InGaZnO thin film transistor *Appl. Phys. Lett.* **99** 082104
[9] Jeong J K, Jeong J H, Yang H W, Park J, Mo Y G and Kim H D 2007 High performance thin film transistors with cosputtered amorphous indium gallium zinc oxide channel *Appl. Phys. Lett.* **91** 113505
[10] Ahn S *et al* 2013 Metal oxide thin film phototransistor for remote touch interactive displays *Adv. Mater.* **24** 2631–6
[11] Yabuta H, Sano M, Abe K, Aiba T, Den T, Kumomi H, Nomura K, Kamiya T and Hosono H 2006 High-mobility thin-film transistor with amorphous $InGaZnO_4$ channel fabricated by room temperature rf-magnetron sputtering *Appl. Phys. Lett.* **89** 112123
[12] Park J *et al* 2008 High-performance amorphous gallium indium zinc oxide thin-film transistors through N_2O plasma passivation *Appl. Phys. Lett.* **93** 053505

[13] Jeon S, Song I, Lee S, Ryu B, Ahn S-E, Lee E, Kim Y, Nathan A, Robertson J and Chung U I 2014 Origin of high photoconductive gain in fully transparent heterojunction nanocrystalline oxide image sensors and interconnects *Adv. Mater.* **26** 7102–9

[14] Chong E, Jo K C and Lee S Y 2010 High stability of amorphous hafnium–indium–zinc-oxide thin film transistor *Appl. Phys. Lett.* **96** 152102

[15] Avis C and Jang J 2011 High-performance solution processed oxide TFT with aluminum oxide gate dielectric fabricated by a sol–gel method *J. Mater. Chem.* **21** 10649–52

[16] Choi H, Jeon S, Kim H, Shin J, Kim C and Chung U I 2011 Verification of interface state poperties of a-InGaZnO thin-film transistors with and gate dielectrics by low-frequency noise measurements *IEEE Electron Device Lett.* **32** 1083–5

[17] Cheong W S, Shin J H, Chung S M, Hwang C S, Lee J M and Lee J H 2012 Current stress induced electrical instability in transparent zinc tin oxide thin-film transistors *J. Nanosci. Nanotechnol.* **12** 3421–4

[18] Luo D, Xu H, Li M, Tao H, Wang L, Peng J and Xu M 2014 Effects of etching residue on positive shift of threshold voltage in amorphous indium–zinc-oxide thin-film transistors based on back-channel-etch structure *IEEE Trans. Electron Device Lett.* **61** 92–7

[19] Choi H, Jeon S, Kim H, Shin J, Kim C and Chung U I 2012 The impact of active layer thickness on low-frequency noise characteristics in InZnO thin-film transistors with high mobility *Appl. Phys. Lett.* **100** 173501

[20] Jeong J K, Yang H W, Jeong J H, Mo Y G and Kim H D 2008 Origin of threshold voltage instability in indium–gallium–zinc oxide thin film transistors *Appl. Phys. Lett.* **93** 123508

[21] Nomura K, Kamiya T and Hosono H 2012 Effect of diffusion of hydrogen and oxygen on electrical properties of amorphous oxide semiconductor, In–Ga–Zn-O, ECS *J. Solid State Sci. Technol.* **2** 5–8

[22] Kamiya T and Hosono H 2010 Material characteristics and applications of transparent amorphous oxide semiconductors *NPG Asia Mater.* **2** 15–22

[23] Park S-H, Cho D-H, Hwang C-S, Yang S, Ryu M K, Byun C-W, Yoon S M, Cheong W-S, Cho K I and Jeon J-H 2009 Channel protection layer effect on the performance of oxide TFTs *ETRI J.* **31** 653–9

[24] Kamiya T and Hosono H 2013 Roles of hydrogen in amorphous oxide semiconductor *ECS Trans.* **54** 103–13

[25] Tsao S W, Chang T C, Huang S Y, Chen M C, Chen S C, Tsai C T, Kuo Y J, Chen Y C and Wu W C 2010 Hydrogen-induced improvements in electrical characteristics of a-IGZO thin-film transistors *Solid-State Electron.* **54** 1497–9

[26] Hanyu Y, Domen K, Nomura K, Hiramatsu H, Kumomi H, Hosono H and Kamiya T 2013 Hydrogen passivation of electron trap in amorphous In–Ga–Zn-O thin-film transistors *Appl. Phys. Lett.* **103** 202114

[27] Noh H-K, Park J-S and Chang K J 2013 Effect of hydrogen incorporation on the negative bias illumination stress instability in amorphous In–Ga–Zn-O thin-film-transistors *J. Appl. Phys.* **113** 063712

[28] Young C D, Zhao Y, Heh D, Choi R, Lee B and Bersuker G 2009 Pulsed–methodology and its application to electron-trapping characterization and defect density profiling *IEEE Trans. Electron Device Lett.* **56** 1322–9

[29] Kim T *et al* 2016 Pulse *I*–*V* characterization of a nanocrystalline oxide device with sub-gap density of states *Nanotechnology* **27** 205203

[30] Young C D *et al* 2005 Ultra-short pulse current–voltage characterization of the intrinsic characteristics of high-κ devices *Japan. J. Appl. Phys.* **44** 2437–40

[31] Heh D, Young C D and Bersurker G 2008 Experimental evidence of the fast and slow charge trapping/detrapping processes in high-k dielectrics subjected to PBTI stress *IEEE Electron Device Lett.* **29** 180–2

[32] Shen C, Li M F, Wang X P, Yee-Chia Y and Kwong D L 2006 A fast measurement technique of MOSFET I_d–V_g characteristics *IEEE Electron Device Lett.* **27** 55–7

[33] Lee S *et al* 2010 Extraction of subgap density of states in amorphous InGaZnO thin-film transistors by using multifrequency capacitance–voltage characteristics *IEEE Electron Device Lett.* **31** 231–3

[34] Jang J, Kim J, Bae M, Lee J, Kim D M, Kim D H, Lee J, Lee B-L, Koo B and Jin Y W 2012 Extraction of the sub-bandgap density-of-states in polymer thin-film transistors with the multi-frequency capacitance–voltage spectroscopy *Appl. Phys. Lett.* **100** 133506

[35] Lee Y, Kang C, Jung U, Kim J, Hwang H, Chung H, Seo S, Choi R and Lee B 2011 Fast transient charging at the graphene/SiO_2 interface causing hysteretic device characteristics *Appl. Phys. Lett.* **98** 183508

[36] Lee J-M, Cheong W-S, Hwang C-S, Cho I-T, Kwon H-I and Lee J-H 2009 Low-frequency noise in amorphous indium–gallium–zinc-oxide thin-film transistors *IEEE Electron Device Lett.* **30** 505–7

[37] Cho I-T, Cheong W-S, Hwang C-S, Lee J-M, Kwon H-I and Lee J-H 2009 Comparative study of the low-frequency-noise behaviors in a-IGZO thin-film transistors with Al_2O_3 and Al_2O_3/SiN_x gate dielectrics *IEEE Electron Device Lett.* **30** 828–30

[38] Jeon S, Kim S I, Park S, Song I, Park J, Kim S and Kim C 2010 Low-frequency noise performance of a bilayer InZnO–InGaZnO thin-film transistor for analog device applications *IEEE Electron Device Lett.* **31** 1128–30

[39] Choi H, Jeon S, Kim H, Shin J, Kim C and Chung U I 2012 The impact of active layer thickness on low-frequency noise characteristics in InZnO thin-film transistors with high mobility *Appl. Phys. Lett.* **100** 173501